matic-hydrogenation side reaction is possible for MBA and MHQ because, as shown in Figure 5B, evolution of molecular hydrogen competes with the hydrodesulfurization reaction; in contrast the desulfurization of PFT was uncomplicated because it took place at potentials where only minute amounts of molecular hydrogen were present. It appears likely that the alkyl group remained on the surface, since, in the chemisorbed state, cleavage of the alkyl C–S bond has been found to occur with greater difficulty than cleavage of the aromatic C–S bond (*8–11*). If pendant alkyl groups were detached from the sulfur anchor, these would have been readily detected. In addition, voltammetric and coulometric analysis of the surface following hydrodesulfurization indicated that the surface consisted of species more complex than H_2S. That is, if all the organic moieties (aromatic or alkyl) had been cleaved from the sulfur anchor, only H_2S would have remained on the surface and electrochemistry characteristic of chemisorbed hydrogen sulfide would have been observed (*7–11*), contrary to what was actually found.

ACKNOWLEDGMENT

Discussions with Manuel M. Baizer were very helpful and greatly appreciated.

Registry No. PFT, 771-62-0; MHQ, 2889-61-4; MBA, 147-93-3; hydroquinone, 123-31-9; benzoquinone, 106-51-4; benzoic acid, 65-85-0; platinum, 7440-06-4.

LITERATURE CITED

(1) Soriaga, M. P.; Hubbard, A. T. *J. Am. Chem. Soc.* **1982**, *104*, 2735.
(2) Soriaga, M. P.; Hubbard, A. T. *J. Am. Chem. Soc.* **1982**, *104*, 2742.
(3) Soriaga, M. P.; Hubbard, A. T. *J. Am. Chem. Soc.* **1982**, *104*, 3937.
(4) Soriaga, M. P.; Wilson, P. H.; Hubbard, A. T.; Benton, C. S. *J. Electroanal. Chem.* **1982**, *142*, 317.
(5) Soriaga, M. P.; Binamira-Soriaga, E.; Hubbard, A. T.; Benziger, J. B.; Pang, K. W. P. *Inorg. Chem.* **1985**, *24*, 65.
(6) Soriaga, M. P.; White, J. H.; Song, D.; Hubbard, A. T. *J. Phys. Chem.* **1984**, *88*, 2285.
(7) Soriaga, M. P.; White, J. H.; Song, D.; Chia, V. K. F.; Arrhenius, P. O.; Hubbard, A. T. *Inorg. Chem.* **1985**, *24*, 73.
(8) Soriaga, M. P.; Stickney, J. L.; Hubbard, A. T. *J. Mol. Catal.* **1983**, *21*, 211.
(9) Soriaga, M. P.; Stickney, J. L.; Hubbard, A. T. *J. Electroanal. Chem.* **1983**, *144*, 207.
(10) Soriaga, M. P.; Hubbard, A. T. *J. Phys. Chem.* **1984**, *88*, 1758.
(11) Soriaga, M. P.; Hubbard, A. T. *J. Electroanal. Chem.* **1983**, *159*, 101.
(12) Hubbard, A. T. *CRC Crit. Rev. Anal. Chem.* **1973**, *3*, 201.
(13) White, J. H.; Soriaga, M. P.; Hubbard, A. T. *J. Electroanal. Chem.* **1984**, *177*, 89.
(14) Hubbard, A. T. *Acc. Chem. Res.* **1980**, *13*, 177.
(15) Ishikawa, R. M.; Katekaru, J. Y.; Hubbard, A. T. *J. Electroanal. Chem.* **1978**, *86*, 271.
(16) Hubbard, A. T. et al. *J. Electrochem. Chem.* **1984**, *168*, 43.
(17) Conway, B. E.; Angerstein-Kozlowska, H.; Sharp, W. A.; Criddle, E. E. *Anal. Chem.* **1973**, *45*, 1331.
(18) Alcalay, W. *Helv. Chim. Acta* **1947**, *30*, 578.
(19) *Fatiadi*, A. J.; Sager, W. F. *Org. Synth.* **1973**, *5*, 595.
(20) Wagenknecht, J. H.; Baizer, M. M.; Chruma, J. L. *Synth. Commun.* **1972**, *2*, 215.
(21) Breiter, M. W. *Electrochemical Processes in Fuel Cells*; Springer-Verlag: New York, 1969.
(22) Reid, E. E. *Organic Chemistry of Bivalent Sulfur, Vol. VI*; Chemical Publishing: New York, 1958; p 334.

RECEIVED for review December 2, 1985. Resubmitted July 18, 1986. Accepted July 18, 1986. Acknowledgment is made to the U.S. Department of Energy, Office of Basic Energy Sciences, Division of Materials Sciences, for support of this research.

Development of Extended X-ray Absorption Fine Structure Spectroelectrochemistry and Its Application to Structural Studies of Transition-Metal Ions in Aqueous Solution

Howard D. Dewald, J. W. Watkins II, R. C. Elder,* and William R. Heineman*

Department of Chemistry, University of Cincinnati, Cincinnati, Ohio 45221-0172

Extended X-ray absorption fine structure (EXAFS) measurements were performed on solutions of various transition-metal complexes. Electrochemical methods were used to generate and maintain the materials in a chosen oxidation state. A spectroelectrochemical cell was constructed with a reticulated vitreous carbon electrode and followed the basic design of an optically transparent thin-layer electrochemical cell. Cell performance was tested on ferrocyanide with chronoamperometry, chronoabsorptometry, and cyclic voltammetry. X-ray absorption spectra of cobalt(III/II) sepulchrate were examined in a potentiostatic study. Fluorescence EXAFS spectra of $Ru(NH_3)_6^{3+}$ were evaluated for sensitivity enhancement as a function of concentration. Cytochrome *c* spectra have been recorded and gave a Fe(III)–N distance of 1.97 Å and a Fe(II)–N distance of 1.99 Å.

Many structural questions of importance in chemistry involve materials that cannot be made crystalline, e.g., amorphous solids and aqueous solutions. The study of these systems was hindered previously by the lack of a technique for determination of local structures. Major advances in the development of synchrotron radiation (*1*) as a source of X-ray photon flux for absorption spectroscopy and a reinterpretation of the extended X-ray absorption fine structure (EXAFS) phenomenon (*2–4*) have made structural studies of ions in solution relatively straightforward (*5–11*). The element specificity of the EXAFS technique allows its application to moderately dilute solutions ($\sim 10^{-2}$ M).

The information contained in EXAFS spectra includes the oxidation state of an absorbing atom, the type and number of atoms surrounding the absorbing atom, and the corresponding bond lengths. Furthermore, absorption features of different elements are well-separated in energy, and thus it is possible to probe the environment of specific elements in a complex sample. Electrochemical methods offer a convenient means for generating complexes in a chosen oxidation state for study through rapid electrolysis.

Basically, in the X-ray absorption experiment an accurate measurement is made of the absorption coefficient, μ, near a particular absorption edge as a function of the photon energy

0003-2700/86/0358-2968$01.50/0 © 1986 American Chemical Society

below and above the ionization threshold. Transitions from a given electron core level to empty valence levels can produce spectral structure near the edge characteristic of the local symmetry and electronic configuration of the atom; transitions to the continuum give rise to oscillations (wiggles) in the absorption coefficient out to as much as 1000 eV above the threshold. The EXAFS function, χ, is the oscillatory part of the absorption coefficient compared to the smoothly varying background, μ_s, normalized by the free atom absorption coefficient, μ_0: $\chi \equiv (\mu - \mu_s)/\mu_0$.

The prevailing physical explanation for the oscillations rests on a photoelectron wave interference pattern. As the energy of the incident photons is varied, the wavelength of the ejected photoelectron changes. Constructive or destructive interference of the wave leaving the absorber occurs with the wave backscattered by surrounding atoms. The constructive interference patterns add, giving a higher transition probability (absorption coefficient) than destructive interference. Sayers et al. (*12*) show how this intereference phenomenon can approximate the EXAFS and be analyzed to obtain structural parameters including interatomic distances and coordination numbers. The basic derived expression can be written as

$$\chi(k) = \sum_j \frac{N_j |f_j(k,\pi)| e^{-2k^2\sigma_j^2}}{kR_j^2} \sin [2kR_j + \alpha_j(k)] \quad (1)$$

The summation is over all coordination shells of scattering atoms. N_j is the number of atoms at a distance R_j in shell j. The electron backscattering amplitude is given by $|f_j(k, \pi)|$ and $\alpha_j(k)$ is the total absorber and scatterer phase-shift function. The photoelectron wave vector is represented as k. The EXAFS is damped by the Debye–Waller related exponential term due to thermal vibrations and/or static disorder. Comprehensive reviews of EXAFS theory and applications are available (*13–18*).

The class of chemical reactions studied most frequently is homogeneous solution reactions. In order to determine the effect of structure changes on reactivity (*19*), it is necessary to know the structures of the reactants in solution. The Marcus–Hush theory (*20–22*) of electron transfer reaction rates requires a calculation of the Franck–Condon barrier associated with changing metal–ligand bond distances on changing oxidation state. Unfortunately, few solution bond distance data have been available. Generally, the solid-state bond distances have been determined by X-ray crystallography and assumed to be freely transferable to solution. The obvious preference would be to have the solution determination of bond distances, as crystal data can vary for a given ion due to differences in counter ions, hydration, or packing forces. Recently, bond distance data for a number of redox couples of simple transition-metal complexes have been obtained from solution EXAFS (*10*). Electrochemical generation of similar couples and subsequent X-ray absorption analysis in situ is direct and offers several advantages. The addition of chemical reducing or oxidizing agents can make the chemistry more complicated and can add an unwanted background to the EXAFS spectrum. Oxygen leaks and the problems of "bleaching" from hydrated electrons produced in samples exposed to the high X-ray flux can cause loss in control of oxidation state; an electrochemical cell maintained at the proper potential throughout the X-ray absorption experiment should maintain the desired redox state for an electroactive material.

Techniques have been developed that combine electrochemistry with spectroscopic measurements throughout the spectrum of electromagnetic radiation (*23*). EXAFS spectroscopy is well-suited for these spectroelectrochemical systems, since the photon probe can penetrate cell windows, electrode materials, and electrolyte solution, while providing structural information about electroactive species in solution.

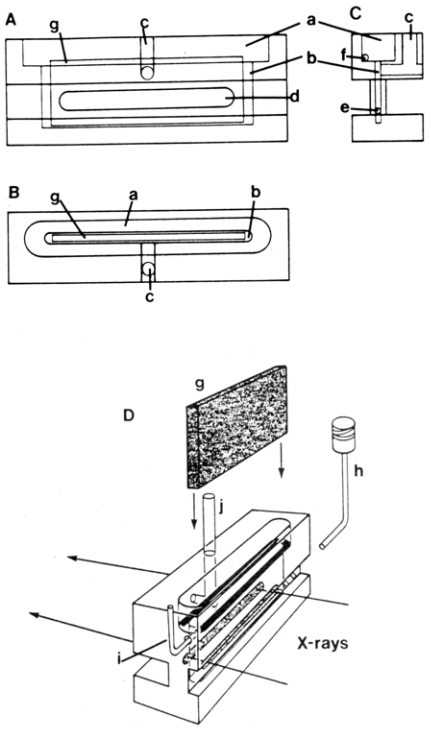

Figure 1. EXAFS spectroelectrochemical cell: (A) front view, (B) top view, (C) side view, (D) assembly; (a) auxiliary electrode compartment, (b) working electrode well, (c) reference electrode compartment, (d) X-ray window, (e) inlet port, (f) auxiliary electrode lead, (g) RVC working electrode, (h) Pt syringe needle inlet and electrical contact, (i) Pt wire auxiliary electrode, (j) Ag/AgCl (3 M NaCl) reference electrode.

Recent reports have shown the diversity of interest in combining in situ electrochemical steps with X-ray absorption spectroscopy for the study of metal passivation (*24*, *25*) and inclusion of metallic clusters in organic conducting polymers (*26*). The first reports from this laboratory described an initial EXAFS thin-layer spectroelectrochemical cell design and the structure analysis of the iron(II/III) cyanide couple (*27*, *28*). We report here the results obtained using a cell with increased electrolytic efficiency and decreased background X-ray absorption and scattering. A spectropotentiostatic study of the cobalt(II/III) sepulchrate system and structure study of cytochrome *c* are presented.

EXPERIMENTAL SECTION

Electrochemical Cell Design. The construction of the spectroelectrochemical cell is shown in Figure 1. The body was machined from Plexiglas G. The outer cell dimensions (l = 45 mm, w = 12.5 mm, h = 20 mm) fit restrictions of the sample chamber of the EXAFS detector. Electrode compartments were milled from the top face. First, the auxiliary electrode compartment (a) was cut. Next, a well (b), centered below the auxiliary electrode compartment, was cut for the working electrode. The reference electrode compartment (c) was connected to the well through a hole drilled in the top face and then at a right angle through the back face. The X-ray window (d) was machined through the front and back faces in two processes. On both sides a channel was cut the full length of the cell near its base. Neither channel cut through to the previously drilled well. A cut was made through the well, centered in the channels, to define the X-ray window (l = 30 mm, h = 3 mm). Two additional small holes were drilled to accept the inlet port (e) and auxiliary electrode lead (f).

The cell was assembled with reticulated vitreous carbon (RVC; ERG, Inc., Oakland, CA; 2 × 3 S; 100 ppi; l = 34 mm, w = 2.5 mm, h = 14 mm) as the working electrode (g). A platinum syringe needle (Hamilton Co., Reno, NV, No. 90518) was bent and pushed into the RVC from the right side, serving both as the filling port and the electrical contact (h). The auxiliary electrode (i) was a 20-gauge platinum wire shaped like an opened paper clip and

encased in an ion-exchange tubing (Nafion 815X, Perma Pure Product, Inc., Toms River, NJ). The auxiliary electrode was placed through the left side hole and positioned along the base of the compartment surrounding the RVC which projected 3 mm into the compartment. Bubbles produced at the auxiliary electrode were channelled through the tubing to the left end of the cell. The ion-exchange tubing also served as a separator between electrodes. The reference electrode (j) was Ag/AgCl (3 M NaCl). The auxiliary electrode compartment cover and the X-ray window cover material were both 0.0005-in. polyimide Kapton tape (3 M, St. Paul, MN).

X-ray Methods. X-ray spectra were measured at beam line IV-3 at Stanford Synchrotron Radiation Laboratory (SSRL). Radiation from the Stanford Positron Electron Accelerating Ring (SPEAR) at an electron energy of 3.0 GeV and current of 80–30 mA was monochromated by a Si(220) double crystal. Higher order harmonics were rejected by "detuning" the crystals, rotating one crystal out of precise alignment of the Bragg planes, to about 50% of the maximum intensity. Incident and transmitted photons were monitored via nitrogen-filled ionization chambers placed before and after the sample, respectively. A set of tantalum slits placed before the first ion chamber was used to mask the beam size to 2 mm × 15 mm. The sample was oriented at 45° with respect to the X-ray beam axis within a sample box, which contained helium to minimize air scattered radiation. A fluorescence detector (EXAFS Co., Seattle, WA) incorporated an argon-filled ionization chamber that was positioned at 90° with respect to the X-ray beam. The fluorescence X-rays passed through a filter, chosen to separate the desired fluorescent Kα photons from the incident X-rays, located on the inside of a Soller-type slit assembly (*29*). Monochromator motor movement and counting electronic circuitry were controlled by a PDP 11/34 computer with SSRL RSX-11M EXAFS data collection software. Wavelength calibration was obtained by measurement of spectra of powdered metal samples (vide infra).

Absorption edge spectra were accumulated typically in 0.5-eV steps with a counting time of 1 s/step over a 40-eV range about the metal K absorption edge. Full EXAFS spectra were measured in three segments. The pre-edge region was measured in 40 equal steps with a counting time of 1 s/step starting 400 eV before the absorption edge; the edge region was collected typically over a 40-eV range about the edge value in 0.2-eV steps for a count time of 1 s/step; the EXAFS region was collected usually in 220 points at evenly spaced intervals in k space with integration times of 1–12 s out to a maximum of k = 16.5 for solid samples or k = 13 for solution samples. Usually three spectra were recorded on solids and five spectra for solutions.

Electrochemical Methods. Cyclic voltammetric and chronoamperometric/coulometric characterization of the spectroelectrochemical cell and samples was performed with a CV-27 voltammograph (Bioanalytical Systems, Inc., West Lafayette, IN). These preliminary electrochemical experiments, which are performed in the laboratory in Cincinnati, allow the determination of the conditions necessary to reduce or oxidize the species of interest during the X-ray experiments at SSRL. During an experimental run at SSRL, an external digital voltmeter was employed with the potentiostat in order to monitor current and measure the applied potential to 0.1 mV simultaneously.

Visible Absorption Methods. Chronoabsorptometric characterization of the spectroelectrochemical cell was performed with a Cary 210 spectrophotometer (Varian Associates, Inc., Palo Alto, CA). A 1-s period and 1-nm bandwidth were used. Strips of black PVC insulating tape covered the cell body, except the spectral window, to mask the light beam. Transparent tape served as the window cover material and was secured against the walls *inside* the working electrode well. An identical cell was placed in the reference beam. A Plexiglas platform was constructed to position the cells in the sample compartment.

EXAFS Data Analysis. Programs used for EXAFS analysis are local modifications of programs originating with Hodgson's group (*30*, *31*). Only fluorescence data were used in the analysis because the increased sensitivity in this mode is necessary for the relatively dilute solutions used in the electrochemical EXAFS experiments (*32*). Preliminary processing involves a calibration procedure to convert the data recorded in monochromator motorsteps to a function of energy, based on a single-point method which uses the known energy associated with the edge position of the metal calibrant. All equivalent spectra for a particular sample are then averaged, and any "glitches" in the data, due to multiple plane diffraction from the monochromator crystals or other aberrant sources, can be removed.

EXAFS, χ, is isolated by subtraction of the smooth fluorescence expected for an isolated absorber atom, approximated by a three-segment cubic spline, and normalization using a Victoreen (*3*) function. Next, the photon energy is converted into a photoelectron wave vector, $k = [2m(E - E_0)/\hbar^2]^{1/2}$, where E_0 is the onset energy for the EXAFS and m is the mass of the electron. After conversion to k space (frequency, Å^{-1}) the data are multiplied by k^2 to aid in the visualization of χ at high k. The modulation of the absorption coefficient, in the form of χ vs. k, is Fourier transformed to R space (distance, Å) to give a radial structure function with peaks corresponding to absorber–scatterer pairs, but phase shifted. For the purpose of curve-fitting techniques, the frequency component of the EXAFS data, corresponding to the desired absorber–scatterer pair(s), is obtained with an inverse transform of the isolated peak(s) using a square window function.

Structural parameters, interatomic distance and coordination number, were obtained using both theoretical and empirical methods of curve fitting. For empirical curve fitting, solid samples of the solution species of interest were used as model compounds. Transferability of amplitudes and phases is assumed in the empirical approach. The Fourier-filtered EXAFS from the solid was fit to a parameterized form of the EXAFS expression

$$\chi(k) = C_1 \exp(C_2 k^2) \sin(C_4 + C_5 k + C_6 k^2)/k^{C_3} \qquad (2)$$

to obtain values for C_1–C_6. Parameters C_2, C_3, C_4, and C_6 are characteristic of the absorber–scatterer pair and as such should describe the absorber–scatterer pair in the solution species. Interatomic distance and coordination number for the solution species were determined by varying the C_1 and C_5 parameters in a nonlinear least-squares process while the remaining parameters were held constant. The bond distance was calculated from $R_{unk} = R_{model} + [C_{5_{unk}} - C_{5_{model}}]/2$ and the number of scatterer atoms as $N_{unk} = N_{model}[C_{1_{unk}} R_{unk}^2]/[C_{1_{model}} R_{model}^2]$.

In theoretical curve fitting, ab initio calculations of amplitude and phase functions were taken from the literature (*33*). The form of the equation for theoretical fits is given as

$$\chi(k) = C_1 \exp(C_2 k^2)\, F(k) \sin(C_3 k + \phi_T)/k \qquad (3)$$

where $F(k)$ is the amplitude function and ϕ_T is the total phase. Additionally, the value of the threshold energy, E_0 (as used above to define k) is an adjustable parameter in the fitting procedure. E_0 and parameters C_1, C_2, and C_3 were varied in the analysis. The bond distance was obtained from the relation $R = C_3/2$ and the coordination number as $N = 2C_1R^2$. In both curve-fitting techniques a goodness of fit or agreement factor was calculated to show the success of the fit to the experimental data.

Materials and Sample Preparation. The following reagents were obtained commercially and used as received: cobalt(III) sepulchrate trichloride (95%), hexammineruthenium(III) chloride (99%) (Aldrich Chemical Co., Milwaukee, WI); potassium ferrocyanide (Fisher Scientific Co.); 2,6-dichlorophenolindophenol sodium salt (Fluka Chemical Corp., Hauppauge, NY); sodium acetate anhydrous (MCB, Cincinnati, OH); and cytochrome *c* (from horse heart, Type VI, 98%, Sigma Chemical Co., St. Louis, MO). Solutions of cobalt(II) sepulchrate, hexammineruthenium(II), ferricyanide, and reduced cytochrome *c* were generated electrochemically.

Solutions 1 M in sodium acetate as the supporting electrolyte were prepared with distilled water. One-milliliter tuberculin syringes were used to fill the electrochemical cell. Air bubbles were dislodged from the RVC by tapping the cell on the lab bench.

Solid samples for the X-ray experiments were prepared by mixing the material for study with Li_2CO_3, as a diluent, and grinding with mortar and pestle to a homogeneous powder. Samples were packed into an aluminum sample holder (sample cavity: w = 28 mm, d = 1 mm, h = 3 mm) and sealed with Kapton tape windows. In all cases the product of the absorption coefficient and the sample thickness, $\Delta\mu x$, was less than 1.0 to avoid any bias in the subsequent calculation of coordination numbers, the so-called "thickness effect" (*34*).

Table I. Transmittance[a] of EXAFS Spectroelectrochemical Cell Components and Cells

energy, keV	H_2O (ρ = 0.997, τ = 0.25)	Mylar[b] ($C_{11}H_{11}O_5$, ρ ~ 1.4, τ = 0.0127)	Kapton[c] ($C_{22}H_{10}O_5N_2$, ρ = 1.42, τ = 0.00127)	Au[d,e] (ρ = 19.29, τ = 0.000 33)	RVC C (ρ = 0.048, τ = 0.25)	RVC[f] cell
6	0.00218	0.750	0.974	0.812	0.880	0.00182
8	0.0760	0.886	0.992	0.852	0.948	0.0709
10	0.265	0.939	0.994	0.892	0.973	0.255
15	0.659	0.980	0.998	0.897	0.990	0.650
20	0.817	0.990	0.999	0.922	0.995	0.811
30	0.910	0.995	0.999	0.962	0.997	0.906

[a] $I/I_0 = \exp[-\tau\rho\sum_i M_i(\mu/\rho)_i]$; τ = thickness (cm), ρ = density (g/cm^3), M_i = mass fraction of element i, $(\mu/\rho)_i$ = mass attenuation coefficient of element i (cm^2/g), calculated from Veigele, W. J. *At. Data* **1973**, *5*, 51–111. [b] Polyethylene terephthalate, Du Pont. [c] Polyimide film, Du Pont. [d] $I/I_0 = 0.8 + 0.2\,(\exp[-\tau\rho\,(\mu/\rho)])$; gold minigrid has 80% visible transmission. [e] One layer of 100 lpi gold minigrid. [f] RVC cell: H_2O × Kapton^2 × RVC.

RESULTS AND DISCUSSION

The spectroelectrochemical cell construction followed the basic design of an optically transparent thin-layer electrochemical cell (*35–37*). Reticulated vitreous carbon (RVC) was chosen as the working electrode material because of its composition, special structure, and electrochemical properties (*38*). The X-rays passing through a sample will be attenuated as given by the equation $I = I_0 \exp[-\rho\ \sum_i M_i(\mu/\rho)_i\tau]$ where I is the intensity of the transmitted beam and I_0 is the intensity of the incident beam. M_i is the mass fraction of the absorber i and μ/ρ is the mass attenuation coefficient of the absorber of density ρ and thickness τ for the energy used. RVC, composed solely of carbon, results in less X-ray attenuation as compared to a gold minigrid, which is the commonly used electrode in thin-layer spectroelectrochemical cells. Mylar and Kapton are two common thin-film sample support materials used for retaining liquid, solid, and powder specimens in X-ray absorption holders. The Kapton tape was chosen because of its ease of application and high transmittance. The largest attenuation of X-ray flux is caused by the water. Table I lists calculated X-ray transmittances at several photon energies for both the individual cell components and the entire cell. It should be apparent that without the high intensity of synchrotron radiation (~10^{12} photons s^{-1} mrad^{-1} mA^{-1}, 1% bandwidth^{-1}), measurements, especially at low photon energies (<8 keV), would require an enormous amount of time for sufficient data collection. Additionally, X-ray scatter from a crystalline metal electrode drastically increases the noise in the measured fluorescence signal. With the amorphous RVC, scattering from the electrode is less than from an equal amount of water.

The open-pore structure of RVC allows easy machining into the desired geometric shape. The RVC is mounted into the cell by a snug fit without any adhesive substances, permitting fast replacement of failed electrodes. Electrochemical equilibrium is achieved rapidly, with electrolysis of the solution in the immediate vicinity of the electrode proceeding to completion within a short time. The free void volume of RVC of ca. 97% results in most of the solution being contained inside the electrode, and thus there exists a short average diffusional path to the electrode surface. This is illustrated in Figure 2 by the chronoabsorptometry/chronocoulometry experiment for the oxidation of ferrocyanide. The potential was stepped to generate ferricyanide, which was optically monitored at 420 nm. As shown by the resulting absorbance–time (A–t) curve, the time required for electrolysis of the ferrocyanide is ca. 5 min. Conversion back to the colorless reduced form is equally fast, as indicated by the return potential step.

The chronoamperometric response as a function of concentration for the ferro/ferricyanide system is shown in Figure 3. As the concentration is increased from 1 mM to 100 mM potassium ferrocyanide the time required to achieve complete oxidation increased from 2 min to 10 min, still quite a rapid process. The high currents produced arise from a combination of experimental conditions, viz., large working electrode, high concentration, natural convection near and within the vertically mounted electrode, diffusion through the ion-exchange membrane isolating the auxiliary electrode, and double-layer charging when the potential was stepped from −0.1 V to +0.6 V. Consequently, there is a large power demand from the potentiostat.

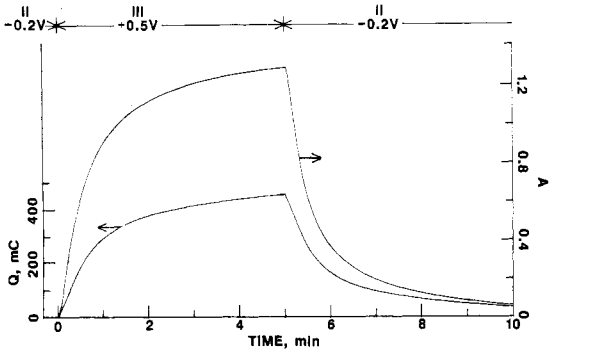

Figure 2. Chronoabsorptometry (A–t) and chronocoulometry (Q–t) of 5.5 mM $K_4Fe(CN)_6$ in 1 M sodium acetate; oxidation at +0.5 V and reduction at −0.2 V vs. Ag/AgCl; absorbance monitored at 420 nm.

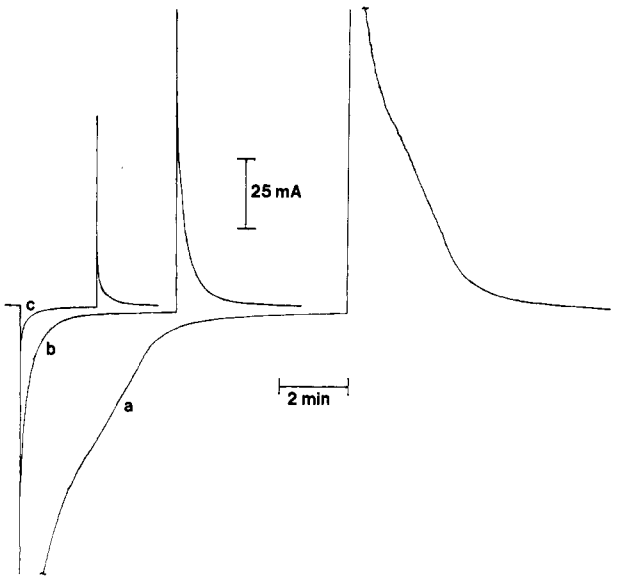

Figure 3. Chronoamperometry of $K_4Fe(CN)_6$ in 1 M sodium acetate: (a) 100 mM, (b) 10 mM, (c) 1 mM; oxidation at +0.6 V and reduction at −0.1 V vs. Ag/AgCl.

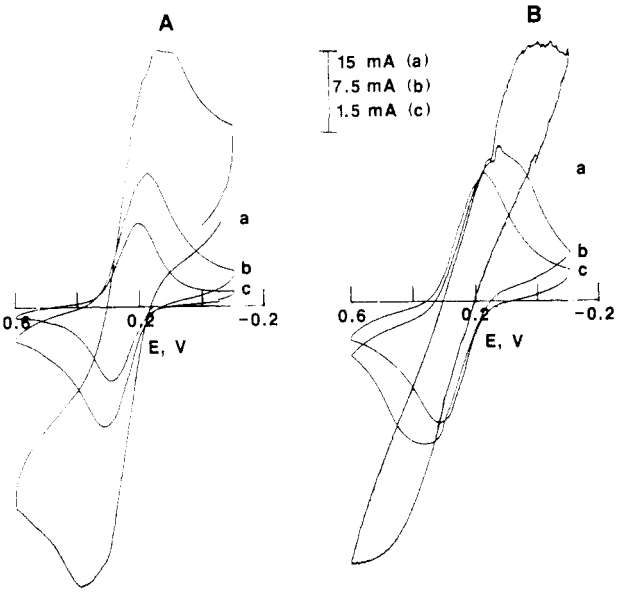

Figure 4. Cyclic voltammetry of $K_4Fe(CN)_6$ in 1 M sodium acetate: (A) 1 mM, (a) 50 mV s^{-1}, (b) 5 mV s^{-1}, (c) 2 mV s^{-1}; (B) 5 mV s^{-1}; (a) 100 mM, (b) 10 mM, (c) 1 mM; scan limits, +0.6 V to −0.1 V vs. Ag/AgCl.

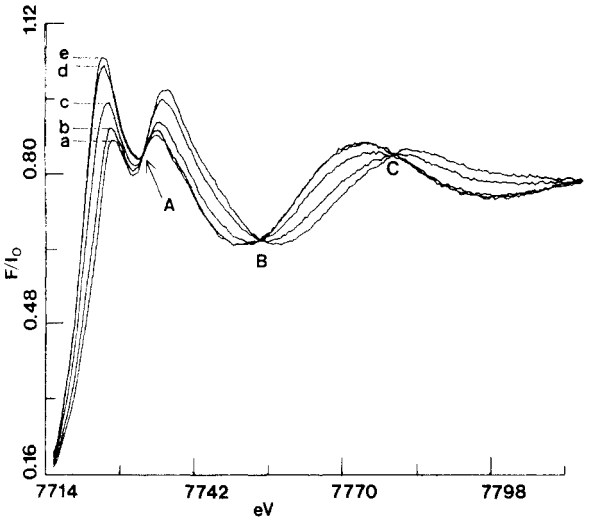

Figure 5. X-ray absorption spectra of 10 mM cobalt sepulchrate in 1 M sodium acetate from potentiostatic experiments: isosbestic points A (7732 eV), B (7754 eV), C (7780 eV); applied potential (a) −0.30 V, (b) −0.58 V, (c) −0.60 V, (d) −0.62 V, (e) −0.80 V vs. Ag/AgCl; fluorescence filter 0.025-mm Fe foil.

The electrolysis times obtained are a 10-fold improvement over previous results (*28*) and are reasonable on the time scale of EXAFS data collection times. This latter point is particularly significant considering limited X-ray beam availability. For example, when a potentiostatic study is made, incorporating several absorption edge scans for each applied potential, an electrolysis time of 30 min/potential step makes the experimental time demands too great.

The geometry of the spectral zone of the cell was dictated by the dimensions and orientation of the X-ray beam. Further, in an attempt to keep the potential and current density the same at all points along the working electrode surface, the oblong arrangement of platinum wire auxiliary electrode around the RVC was chosen. The auxiliary electrode compartment was placed above the spectral zone of the cell and the platinum wire surrounded with ion-exchange tubing. The tubing channelled bubbles to one end of the cell where they escaped to air above the solution. Additionally, the tubing served as a spacer to prevent the two electrodes from shorting. This top/bottom arrangement of electrode compartments is superior to the previous choice of a front/back arrangement (*39*). The planar area of the RVC was thus governed by these design criteria. The RVC electrode thickness was limited by how thin the electrode well in the cell could be machined. (The thinnest workable thickness for RVC is ~0.5 mm.) Optimization of cell thickness is governed by X-ray attenuation (vide supra) and cell resistance as discussed earlier (*28*). The placement of the reference electrode tip was in the upper center of the cell and close to the RVC. The reference electrode is not on a line between the working and auxiliary electrodes, but this did not appear critical to the cell performance.

The high/low concentration condition is a relative term depending on the technique being discussed. While 10 mM is considered to be high by analytical electrochemists, it represents a dilute level (near minimum) to produce a good signal-to-noise ratio in the X-ray absorption experiments (vide infra). The supporting electrolyte (1 M sodium acetate) was needed to minimize potential gradients and was selected for its high X-ray transmittance.

Typical cyclic voltammograms of the cell for ferrocyanide at various scan rates and concentrations are shown in Figure 4. The voltammograms exhibit a characteristic shape with a rapid drop in current to near zero following the peak in each scan direction for the slow scan rates and low concentrations. This is once again indicative of complete electrolysis of the electroactive species. All values of i_{p_a}/i_{p_c} are approximately equal to 1.0 indicating the reversibility of the system and retention of the electroactive material within the cell. The cathodic and anodic peak separation (ΔE_p) is greater than the expected value of 0 V for thin-layer behavior as a result of uncompensated iR drop between the reference electrode and the RVC working electrode. The voltammogram recorded at a scan rate of 2 mV s^{-1} resulted in a peak separation of 80 mV. The peak separation increases with faster scan rates and higher concentration because of the larger currents. The $E^{\circ\prime}$ of the system, calculated as the average of the cathodic and anodic peak potentials, is +0.25 V vs. Ag/AgCl. The cyclic voltammetric behavior is comparable to the common optically transparent electrode (*37*) and is a considerable improvement upon our earlier cell design (*28*).

As compared to gold, RVC displays larger overpotentials for production of H_2 and O_2, thereby extending both the negative and positive ranges. A range about +1.2 V to −1.0 V vs. SCE at pH 7 for RVC has been reported (*38*). In this study we have applied potentials frequently at values of ±1.0 V vs. Ag/AgCl without any difficulty. Additionally, because RVC is inert, strongly acidic or basic solutions have little or no effect on the electrode performance.

As a further evaluation of the cell, a potentiostatic experiment was performed by recording X-ray spectra of cobalt(III) sepulchrate at a series of applied potentials (*23*). The cobalt(III) was converted incrementally from its oxidized to reduced form, as shown in Figure 5. As can be seen, the inflection point for the Co K absorption edge rise shifted 2.4 eV to lower energy upon reduction from Co(III) to Co(II). The isosbestic points A, B, and C are indicative of the presence of only two species in solution. The fact that the isosbestic points are well-maintained over five different potential steps supports this claim. Further, in an experiment performed 6 months previously, spectra were measured on separate 10 mM solutions of cobalt(III) and cobalt(II) sepulchrate. The super position of those two spectra gives the same crossing points as those reported here within ±0.5 eV.

As mentioned earlier, 10 mM solutions are dilute for EXAFS experiments. The effect of a deteriorating signal-to-noise ratio for data collected in both transmission and fluorescence modes for 100–1 mM $Ru(NH_3)_6Cl_3$ is shown in parts A and B, respectively, of Figure 6. The EXAFS

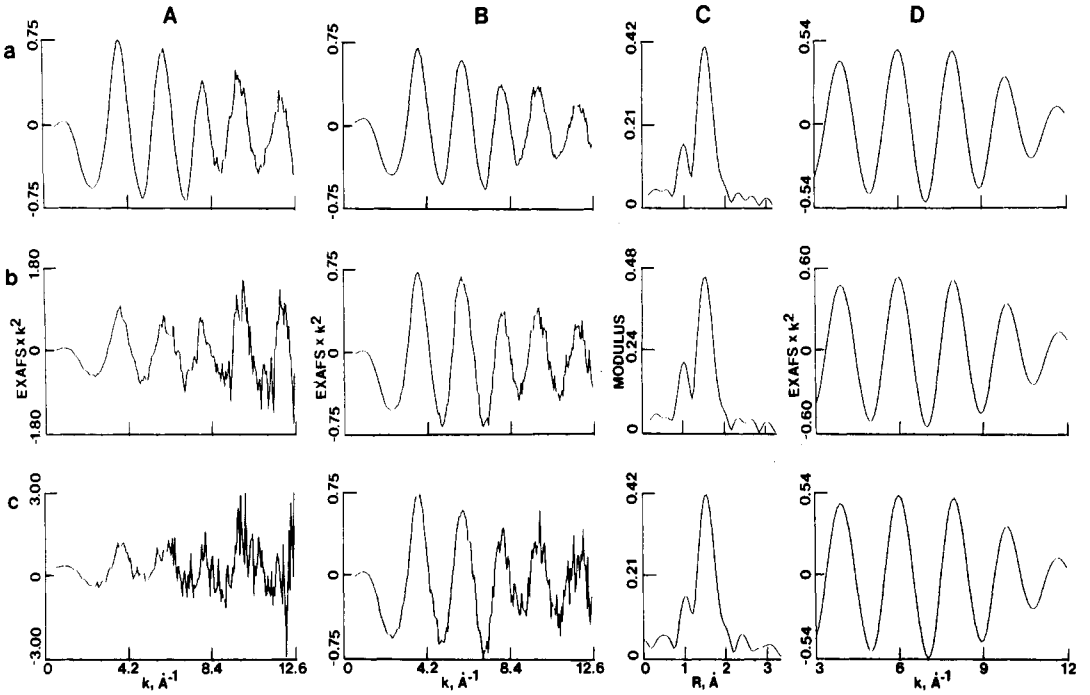

Figure 6. EXAFS spectra of $Ru(NH_3)_6Cl_3$ in 1 M sodium acetate: Concentrations (a) 100 mM; (b) 10 mM; (c) 1 mM; (A) transmission mode; (B) fluorescence mode; (C) Fourier transforms of B, k = 3–12 Å^{-1}, E_0 = 22139.3 eV; (D) Fourier filters of C, R = 1.239–2.129 Å; applied potential +0.2 V vs. Ag/AgCl. Fluorescence filter 0.025-mm Mo foil.

Table II. EXAFS Empirical Curve-Fitting for $Ru(NH_3)_6Cl_3$ Fluorescence Data Ru-N[a]

concn, mM	R,[b] Å	N[c]	F[d]
100	2.091	6.9	0.19
10	2.088	7.6	0.23
1	2.093	7.3	0.20

[a] E_0 = 22139.3 eV; Fourier transform, k = 3–12 Å^{-1}; Fourier filter, R = 1.24–2.13 Å; curve fit, k = 4–11 Å^{-1}. [b] Model $Ru(NH_3)_6Cl_3$: R = 2.104 Å, N = 6, F = 0.07. [c] N = coordination number; uncertainty ± 20%. [d] F = goodness of fit = $[\sum k^6(\chi_{obsd} - \chi_{calcd})^2]^{1/2}/N$, where N is the number of data points.

multiplied by k^2 have been plotted vs. k. The decrease in quality for the transmission data is much more pronounced (*40*). The Fourier transform of the fluorescence data (Figure 6C) exhibits one major peak for the Ru–N absorber–scatterer pair. Back transformation of the peak generated the Fourier-filtered data shown in Figure 6D. Interestingly, the filtered data for the three concentration levels are nearly indistinguishable. The improvement of the data on filtering results from removal of high-frequency noise components. The results from curve fitting of this filtered data with empirical parameters derived from the solid model are given in Table II.

The curve-fitting results are internally consistent. The EXAFS results are within ±0.02 Å of agreement with crystal structure results. More importantly, the results do not change significantly as the concentration is lowered. Considering these EXAFS results, which are for single scans without the benefit of signal averaging, it appears that ruthenium solutions of 10^{-4} M could be examined readily. This is highly desirable for study of many bioinorganic complexes that exhibit low solubility or for which little sample is available. Also, the problem associated with the high currents that accompany the higher concentrations is minimized.

The calculation of signal-to-noise (S/N) ratios for fluorescence detection is dependent on the method and degree of scatter rejection. Lee et al. (*18*) have given considerable attention to this subject. In practice the first-row transition metals require a higher concentration in order to obtain the same S/N as the higher Z transition metals, as a result of lower fluorescent yields and higher background scatter. For the case of an iron compound, for example, a lower limit of 10^{-3} M solutions is more realistic.

Cytochromes *c* represent one class of bioinorganic complexes of interest. They exhibit a wide range of oxidation–reduction potentials. To understand their chemistry requires knowledge of the changes in structure from one oxidation state to another. The X-ray crystallographic structures of various cytochromes *c* show a histidyl nitrogen and a methionyl sulfur as axial ligands to the iron atom. The differences in redox potentials among the proteins are not due to differences in their ligating atoms, but may arise from differences in their iron–ligand bond distance or orientation. EXAFS is able to detect small structural changes (≥0.01 Å) that might accompany a change in oxidation state or redox potential.

Recent EXAFS work on five structurally homologous high-potential cytochromes *c* indicated no average iron–axial ligand bond length differences greater than 0.03 Å among the series, although significant reduction potential variation was seen (*41*). The work was conducted using chemical reducing and oxidizing agents. Oxidation–reduction midpoint potentials for each cytochrome were determined by titration following the EXAFS experiment. Previously, we have applied spectroelectrochemistry in the visible wavelength region to the study of cytochrome *c* (*36*, *42*). Figure 7 shows the spectra obtained for 10 mM horse heart cytochrome *c* in the fully oxidized and reduced forms using EXAFS spectroelectrochemistry in the presence of 2,6-dichlorophenolindophenol, which functioned as an intermediate electron transfer agent between the electrode and heme protein. Figure 8 presents the Fourier transforms of the spectra of oxidized and reduced cytochrome. The first coordination shell peak representing both the Fe–N and Fe–S interactions occurs at 1.5 Å. The peaks at low values of R are artifacts resulting from series truncation errors and residual low-frequency background. The peaks at longer distances represent noise. The inverse Fourier transform was performed on the isolated first shell from 1.12 to 2.01 Å. Our curve-fitting analyses using ab initio phases and amplitudes give a Fe(III)–N distance of 1.97 Å and a

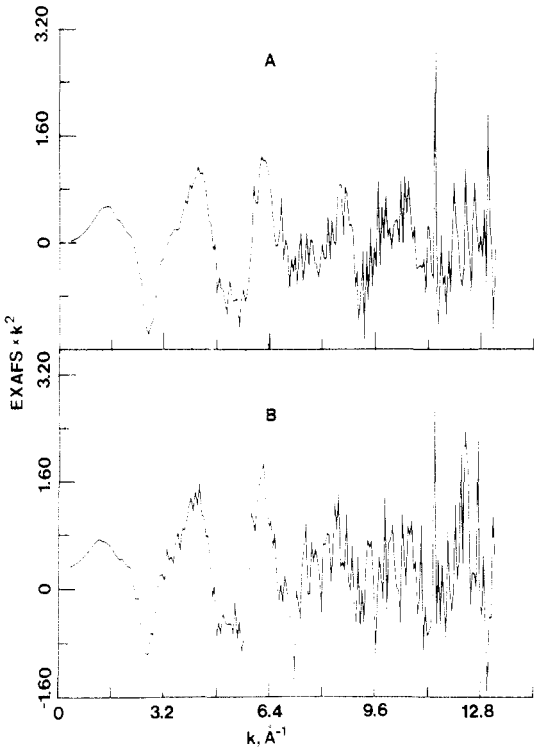

Figure 7. EXAFS spectra of 10 mM horse heart cytochrome *c* in 2 mM 2,6-dichlorophenolindophenol and 1 M sodium acetate: (A) oxidized form, applied potential +0.3 V vs. Ag/AgCl; (B) reduced form, applied potential −0.5 V vs. Ag/AgCl; E_0 = 7130 eV; fluorescence filter 0.05-mm Mn/Cu foil (80% Mn, 20% Cu).

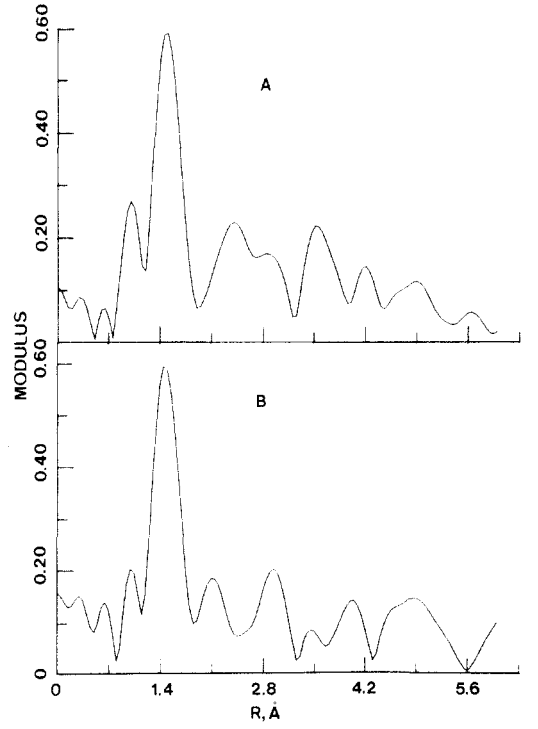

Figure 8. Fourier transforms of EXAFS spectra of 10 mM horse heart cytochrome *c*: (A) oxidized form and (B) reduced form; k = 2–12 Å^{-1}, E_0 = 7130 eV.

Fe(II)–N distance of 1.99 Å. The Fe K absorption edge shifted 1.5 eV to lower energy upon reduction of the cytochrome *c*. These results are in agreement with values determined by Korszun et al. (*41*). For empirical curve-fitting analysis of the single-shell model, the EXAFS of solid cytochrome *c* was Fourier filtered to isolate both the Fe–N and Fe–S interactions. A six-parameter fit was performed on the data using eq 2. For analysis of the solution spectra, only the two variables related to the bond length and coordination number were varied; the shape of the amplitude envelope and total phase shift were fixed. No difference in bond distance was observed for oxidized or reduced cytochrome. The value of the parameter relating bond length between the model and solution samples was unchanged within an experimental error of 0.01 Å. The value of the coordination number decreased to 0.8 of the model. However, some of the decrease may be the result of holding the Debye–Waller factor constant; the environment around the solid would be expected to be different from a dilute solution.

The effect of X-ray irradiation of biological samples has been reported by Chance et al. (*43*). With fluxes of 10^{10}–10^{11} photons s^{-1}, ~2.5 μM s^{-1} hydrated electrons (e^- aq) can be produced in the sample. We observed a 40% reduction of a 10 mM cytochrome *c* sample that was exposed for 6 h to the X-ray beam in the absence of potential control. With the electrochemical cell this problem is avoided by application of a potential that ensures any transiently reduced species is reoxidized rapidly.

In sum, we have been able to demonstrate a powerful new technique of EXAFS spectroelectrochemistry for preparing and characterizing solutions of transition-metal and biological complexes in varied oxidation states. In the process thin-layer spectroelectrochemistry generates and maintains materials in a particular oxidation state easily and quantitatively while X-ray absorption spectra are recorded. The X-ray spectra are analyzed in terms of coordination numbers, interatomic distances, oxidation state, and ligand identity. This hybrid eliminates some weak points of each separate analysis tool, e.g., the lack of definite chemical identification in spectroelectrochemistry and the limited number of stable oxidation states which can be generated by chemical reductants and oxidants for analysis by conventional X-ray absorption spectroscopy.

ACKNOWLEDGMENT

We thank D. M. Caster for aid in data collection and helpful discussions.

Registry No. $Ru(NH_3)_6^{3+}$, 18943-33-4; cobalt(III) sepulchrate, 72496-77-6; cobalt(II) sepulchrate, 63218-22-4; cytochrome *c*, 64479-33-0.

LITERATURE CITED

(1) Hodgson, K. O.; Doniach, S. *Chem. Eng. News* **1978**, *56*(34), 26–37.
(2) Stern, E. A. *Phys. Rev. B* **1974**, *10*, 3027–3037.
(3) Lytle, F. W.; Sayers, D. E.; Stern, E. A. *Phys. Rev. B* **1975**, *11*, 4825–4835.
(4) Stern, E. A.; Sayers, D. E.; Lytle, F. W. *Phys. Rev. B* **1975**, *11*, 4836–4846.
(5) Eisenberger, P.; Kincaid, B. M. *Chem. Phys. Lett.* **1975**, *36*, 134–136.
(6) Sandstrom, D. R.; Dodgen, H. W.; Lytle, F. W. *J. Chem. Phys.* **1977**, *67*, 473–476.
(7) Cramer, S. P.; Gray, H. B.; Dori, Z.; Bino, A. *J. Am. Chem. Soc.* **1979**, *101*, 2770–2772.
(8) Sham, T.-K.; Hastings, J. B.; Perlman, M. L. *J. Am. Chem. Soc.* **1980**, *102*, 5904–5906.
(9) Sham, T.-K.; Brunschwig, B. S. *J. Am. Chem. Soc.* **1981**, *103*, 1590–1591.
(10) Brunschwig, B. S.; Creutz, C.; Macartney, D. H.; Sham, T.-K.; Sutin, N. *Faraday Discuss. Chem. Soc.* **1982**, *74*, 113–127.
(11) Cramer, S. P.; Eidem, P. K.; Paffett, M. T.; Winkler, J. R.; Dori, Z.; Gray, H. B. *J. Am. Chem. Soc.* **1983**, *105*, 799–802.
(12) Sayers, D. E.; Stern. E. A.; Lytle, F. W. *Phys. Rev. Lett.* **1971**, *27*, 1204–1207.
(13) Stern, E. A. *Sci. Am.* **1976**, *234*(4), 96–103.
(14) Eisenberger, P.; Kincaid, B. M. *Science (Washington, D.C.)* **1978**, *200*, 1441–1447.
(15) Cramer, S. P.; Hodgson, K. O. *Prog. Inorg. Chem.* **1979**, *25*, 1–39.
(16) Teo, B.-K. *Acc. Chem. Res.* **1980**, *13*, 412–419.
(17) Koningsberger, D. C.; Prins, R. *TrAC, Trends Anal. Chem.* **1981**, *1*, 16–21.
(18) Lee, P. A.; Citrin, P. H.; Eisenberger, P.; Kincaid, B. M. *Rev. Mod. Phys.* **1981**, *53*, 769–806.
(19) Hupp, J. T.; Weaver, M. J. *J. Phys. Chem.* **1985**, *89*, 2795–2804.
(20) Creutz, C. *Prog. Inorg. Chem.* **1983**, *30*, 1–73.
(21) Endicott, J. *Prog. Inorg. Chem.* **1983**, *30*, 141–187.

(22) Sutin, N. *Prog. Inorg. Chem.* **1983**, *30*, 441-498.
(23) Heineman, W. R. *J. Chem. Educ.* **1983**, *60*, 305-308.
(24) Kordesch, M. E.; Hoffman, R. W. *Nucl. Instrum. Methods Phys. Res., Sect. A* **1984**, *222*, 347-350.
(25) Bosio, L.; Cortes, R.; Defrain, A.; Froment, M. *J. Electroanal. Chem.* **1984**, *180*, 265-271.
(26) Tourillon, G.; Dartyge, E.; Dexpert, H.; Fontaine, A.; Jucha, A.; Lagarde, P.; Sayers, D. E. *J. Electroanal. Chem.* **1984**, *178*, 357-366.
(27) Smith, D. A.; Heeg, M. J.; Heineman, W. R.; Elder, R. C. *J. Am. Chem. Soc.* **1984**, *106*, 3053-3054.
(28) Smith, D. A.; Elder, R. C.; Heineman, W. R. *Anal. Chem.* **1985**, *57*, 2361-2365.
(29) Stern, E. A.; Heald, S. M. *Rev. Sci. Instrum.* **1979**, *50*, 1579-1582.
(30) Eccles, T. K. Ph.D. Dissertation, Stanford University, CA, 1977.
(31) Cramer, S. P. Ph.D. Dissertation, Stanford University, CA, 1977.
(32) Jaklevic, J.; Kirby, J. A.; Klein, M. P.; Robertson A. S.; Brown G. S.; Eisenberger, P. *Solid State Commun.* **1977**, *23*, 679-682.
(33) Teo, B.-K.; Lee, P. A. *J. Am. Chem. Soc.* **1979**, *101*, 2815-2832.
(34) Stern, E. A.; Kim, K. *Phys. Rev. B* **1981**, *23*, 3781-3787.
(35) Murray, R. W.; Heineman, W. R.; O'Dom, G. W. *Anal. Chem.* **1967**, *39*, 1666-1668.
(36) Anderson, C. W.; Halsall, H. B.; Heineman, W. R. *Anal. Biochem.* **1979**, *93*, 366-372.
(37) Norvell, V. E.; Mamantov, G. *Anal. Chem.* **1977**, *49*, 1470-1472.
(38) Wang, J. *Electrochim. Acta* **1981**, *26*, 1721-1726.
(39) Smith, D. A.; Dewald, H. D.; Watkins, J. W.; Heineman, W. R.; Elder, R. C. 167th Meeting of the Electrochemical Society, Toronto, Ont., Canada, May 1985; The Electrochemical Society, Inc.: Pennington, NJ; Abstract 602.
(40) Elder, R. C.; Tepperman, K. G.; Eidsness, M.; Heeg, M. J. Proceedings of Bioinorganic Chemistry of Gold Coordination Compounds. Nov 16-17, 1981, Philadelphia, PA, Smith Kline & French Laboratories, 1983; pp 124-142.
(41) Korszun, Z. R.; Moffat, K.; Frank, K.; Cusanovich, M. A. *Biochemistry* **1982**, *21*, 2253-2258.
(42) Heineman, W. R.; Norris, B. J.; Goelz, J. F. *Anal. Chem.* **1975**, *47*, 79-84.
(43) Chance, B.; Angiolillo, P.; Yang, E. K.; Powers, L. *FEBS Lett.* **1980**, *112*, 178-182.

RECEIVED for review January 17, 1986. Accepted July 18, 1986. Support for this project was provided by National Science Foundation Grant CHE-8401525. Work was done at SSRL, which is supported by the Department of Energy, Office of Basic Energy Sciences, and the National Institutes of Health, Biotechnology Resource Program, Division of Research Resources.

Application of Glutaraldehyde to Amperometric Determination of Protein in Dairy Products

Hiroyuki Ukeda, Eiji Miyazaki, Kiyoshi Matsumoto,* and Yutaka Osajima

Department of Food Science and Technology, Faculty of Agriculture, 46-09, Kyushu University, Fukuoka, 812, Japan

A simple and rapid determination of protein in dairy products utilizing the bifunctional reagent glutaraldehyde is described. The method is based on monitoring oxygen consumed in the reaction of glutaraldehyde with the compound containing amino group as amino acids and protein with a Clark oxygen electrode. The addition of a redox-mediating compound accelerated the rate of oxygen consumption. The current decrease for 3 min was linearly related to glycine in the range 2.2×10^{-4} to 3.3×10^{-3} M. The detection limit was 5.8×10^{-5} M and the relative standard deviation was 1.50% for ten successive assays at the 4.35 mM glycine level. For commercially available dairy products, a good linear relationship ($r = 0.996$) exsisted between the current response by the proposed method and protein content by the Kjeldahl method. The amperometric detection of protein permitted the direct introduction of samples to analysis without a pretreatment procedure. Thus, the method appears to be feasible and practical for the determination of protein in dairy products.

Protein determinations are of great interest in diverse fields, and many methods have been developed, particularly with a view to routine and automated procedures (*1*, *2*). In the field of food technology, however, the Kjeldahl method has been used commonly as a major method. The Kjeldahl method was the first well-known, routine method for protein determination, but of course, it gives positive results for many nitrogen-containing compounds. Obviously, there is a demand for exploring new methods of monitoring proteins. In particular, there is a need for simple, reliable, rapid, and inexpensive methods applicable to small volumes, e.g., for monitoring proteins in food.

In this paper, we propose a new method of determination of protein in dairy products using the bifunctional reagent glutaraldehyde, which is widely used in such diverse fields as enzymology (*3*), electron microscopy (4), and X-ray crystallography (*5*). The method is based on the observation that oxygen in the solution is consumed when glutaraldehyde reacts with the compound containing an amino group such as amino acids and proteins. The oxygen consumption may be due to the formation of dihydropyridine by the interaction of glutaraldehyde with amino groups followed by the oxidation to pyridinium salts. It was recognized, furthermore, that the addition of a redox-mediating compound, that is, mediator (*6*), accelerated the rate of oxygen consumption. To our knowledge, no one has applied glutaraldehyde to the determination of protein. This paper shows the reaction mechanism and the optimization of the new method and its application to dairy products.

EXPERIMENTAL SECTION

Reagent. Glutaraldehyde (70% aqueous solution for biochemistry), vitamin K_3 (2-methyl-1,4-naphthoquinone), 2,6-dichlorophenolindophenol (sodium salt; DCPIP), and phenazine methosulfate (*N*-methylphenazonium methosulfate; PMS) were obtained from Wako Pure Chemical Industry (Osaka, Japan). β-Naphthoquinone-4-sulfonic acid (potassium salt; β-NQ) was purchased from Nakarai Chemical Co. (Kyoto, Japan). Sodium borohydride was obtained from Ishizu Pharmaceutical Co. (Osaka, Japan). All other chemicals were of analytical grade and were used without further purification. All glutaraldehyde solutions were prepared from 70% aqueous solution by diluting with 0.2 M phosphate buffer (pH 8.2), unless otherwise mentioned. Deionized water was used in the preparation of all other solutions.

Apparatus. A ~2-mL cell was used for the determination. The upper opening of the cell was closed with an acrylic resin male capillary, and the side opening contained a Clark oxygen electrode. The Clark oxygen electrode was purchased from Yellow Springs Instrument Co. (Model No. 5331). The current was measured with a laboratory-made instrument which could change the imposed potential from −2.0 V to +2.0 V and could measure the current from 10 nA full scale to 100 μA full scale with five ranges. The potential of the oxygen electrode was fixed at −0.8 V and the other treatments of the electrode were carried out as

0003-2700/86/0358-2975$01.50/0 © 1986 American Chemical Society